Investigation of the interatomic potential using the crystal gamma-ray-induced Doppler-broadening method on oriented Ni single crystals

N. Stritt and J. Jolie
Institut de Physique, Université de Fribourg, Pérolles, CH-1700 Fribourg, Switzerland

M. Jentschel, H. G. Börner, and C. Doll
Institut Laue Langevin, Avenue des Martyrs, Boîte Postale 156X, F-38042 Grenoble Cedéx, France
(Received 1 April 1998; revised manuscript received 20 October 1998)

The gamma-ray-induced Doppler-broadening method, relying on high-resolution gamma-ray spectroscopy, involves direct measurement of the Doppler broadening of gamma rays emitted when nuclei decay in flight following recoil induced by preceding gamma rays. This method is used to study interatomic collisions at low energy in solids and in this way to probe the repulsive interatomic potential. Line shapes of gamma rays, emitted by the recoiling ^{59}Ni isotope after thermal neutron capture in Ni single crystals, were measured and compared to results obtained by molecular dynamics simulations of the slowing down. Several potentials (including different embedded-atom method potentials) are investigated using the observed fine structure of the line shape, which depends on the crystal orientations. From a detailed study of the line shapes measured in two different orientations, a new potential is then derived. [S0163-1829(99)06409-7]

I. INTRODUCTION

The gamma-ray-induced Doppler-broadening (GRID) method is based on the observation of Doppler shifts produced by the motion of emitting nuclei in solid targets.[1] Using thermal neutron capture, a nucleus is excited to an energy equal to the neutron binding energy (typically 9 MeV). The newly formed capture state will then decay by emission of gamma rays. Each emission of a gamma ray induces a recoil to the nucleus. If the nucleus emits a second gamma ray while still in flight, the measured energy of the latter will be Doppler shifted. In the measurement reported here, the recoil energy given to the atom is between 200 and 400 eV. This gives enough recoil to the atom to move several sites away from its equilibrium position and to make collisions with other atoms in the bulk. As the emissions of primary gamma rays, hence the recoil directions, are isotropically distributed, this leads to a Doppler broadening (rather than a Doppler shift) for the measured energy distribution of the gamma rays emitted in flight. The broadened line shape depends on the recoil velocities at the moment of emission of the measured gamma rays. The velocity of the atoms at that time is related to two effects: the lifetime of the nuclear state which gives the time of emission and the slowing down of the atom in the bulk. As the residual recoil velocity depends on the slowing down the nucleus has experienced since the emission of the first gamma ray, the GRID method will give valuable information on the slowing-down process governed by the interatomic potential. The GAMS4 spectrometer, installed at the high-flux reactor of the ILL and designed to measure gamma rays with a resolution of a few eV, can detect the gamma-ray-induced Doppler broadening. With the use of molecular dynamics (MD) simulations which predict the slowing down of atoms in bulk material, the comparison between the theories (given by interatomic potentials) and the measurement (GAMS4 data) can be realized.[2] Knowledge of one of the two unknowns (slowing-down theory or the lifetime value) determining the gamma-ray line shape permits with the GRID data to test the other. As many nickel isotopes and their nuclear state lifetimes are fairly well known and are listed in a recent article,[3] a study of the slowing down as a function of the Ni-Ni interatomic potential is possible from GRID data. It should also be noted that a similar experiment was conducted several years ago with polycrystalline targets and aiming to the determination of the lifetimes of excited nuclear states.[2,4]

As a result of the ordered structure of single crystals, the profile of the line shape should vary for different orientations in between the crystals planes and the spectrometer. Thus the use of single crystals as targets presented in this work permits us to test several orientations. While the nuclear lifetime is independent of the orientation, blocking and/or channeling effects due to the crystal structure of the target influence strongly the exact form of the measured Doppler-broadened line shape. Using the crystal-GRID method, the anisotropy of the slowing-down motion in the crystals becomes observable and is not smeared out like in polycrystalline structures. Therefore, this technique becomes a sensitive tool for the study of the interatomic potentials[5,6] and permits a more complete analysis of the potentials. Theoretical interatomic potentials, such as the Born-Mayer (BM) and Ziegler-Biersack-Littmark (ZBL) type, and potentials derived using the embedded-atom method (EAM) exist and are still being developed. Many of these potentials can reproduce quite well solid-state properties and are usually based on reproduction of crystal constants. In particular, the EAM potentials have been widely used to study a variety of problems including point defect properties,[7] surface relaxation[8] and reconstruction,[9] surface and bulk phonons,[10] liquid structure, thermal expansion,[11] segregation in alloys,[12] grain boundary structure, and mechanical properties[13] and give fairly good results. The purpose of this paper is to test the same interatomic potentials in another energy domain by investigating if the description given by these potentials is adequate for the

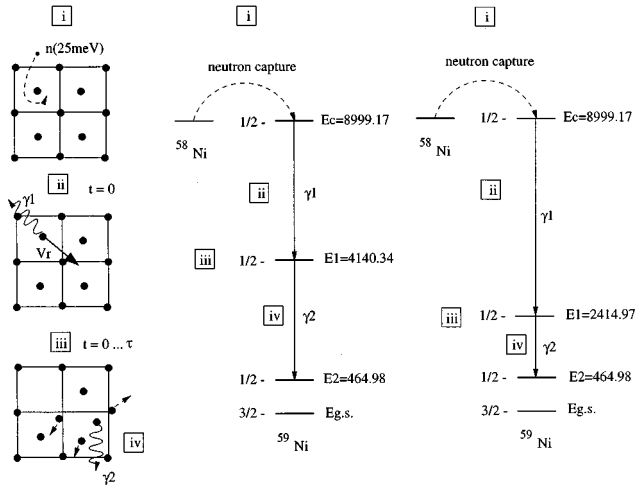

FIG. 1. Description of the nuclear reaction and the nuclear-state levels and transitions of interest for the ^{58}Ni-^{59}Ni isotopes. For simplicity purpose, the movement of the recoiling atom is restricted to one dimension.

slowing down of atoms having a kinetic energy of a few hundred eV. It will then be shown how the matching of the description of the line profiles measured in different orientations of the target allows the determination of a new potential.

II. CRYSTAL-GRID METHOD

The processes involved in the production of a Doppler-broadened gamma-ray line shape are described in Fig. 1. First, (i) neutron capture forms an excited nucleus. The newly formed atom will deexcite by emitting a first gamma ray (ii). This emission will induce a recoil to the nucleus and the atom starts to move in the crystal (iii). If a second gamma ray is emitted during the flight (iv) at a time depending on the nuclear state lifetime (τ), it will be Doppler shifted due to the velocity of the emitting atom. The GAMS4 spectrometer measures the energy of the second gamma ray with respect to a fixed direction and gives valuable information on the gamma-ray line shape. If the recoil is induced by only one primary gamma ray (no cascade), then the recoil energy (E_r) and velocity (v_r) of the atom at the moment of emission are given by

$$E_r=\frac{E_{\gamma_1}^2}{2Mc^2} \quad \text{and} \quad \frac{v_r}{c}=\frac{E_{\gamma_1}}{Mc^2}, \tag{1}$$

with E_{γ_1} the energy of the primary gamma ray, M the mass of the recoiling atom, and c the velocity of light.

The isotope investigated in the present experiment is ^{58}Ni in a natural Ni single crystal. This isotope has a 64.3% natural abundance and has a neutron cross section of 4.6 b. The nuclear reaction involved in the crystal-GRID method analyzed in this work is

$$^{58}_{28}\mathrm{Ni}_{30}+n(25\ \mathrm{meV})\rightarrow{}^{59}_{28}\mathrm{Ni}^{*}_{31}\rightarrow{}^{59}_{28}\mathrm{Ni}_{31}+\gamma. \tag{2}$$

The first reaction is a thermal neutron capture producing the excited ^{59}Ni isotope. After thermal neutron capture, a $1/2^+$ level at 8999.2 keV in ^{59}Ni is populated.[3] This excited level decays by gamma-ray cascades to the ground state. Three levels and Doppler-broadened transitions were chosen to be analyzed by the GAMS4 spectrometer: two for the gamma-ray-induced Doppler broadening and one for the determination of the broadening due to thermal motion. A partial-level scheme showing the ^{59}Ni decay of interest is given in Fig. 1. The levels and transitions studied in this work are summarized in Table I. The first level at 4140 keV decays with a lifetime of 6.5 fs (Ref. 3) via emission of a 3675-keV gamma ray to a long-lived $1/2^-$ state at 465 keV. The second level decays via emission of a 1950-keV gamma ray to the same long-lived state. Formula (1) gives a recoil energy of 215.8 eV for the 3675-keV transition and a recoil energy of 396.5 eV for the 1950-keV transition. The third level at 339 keV used for the determination of the thermal broadening has a long lifetime [98.1 ps (Ref. 3)] and decays to the $3/2^-$ ground state.

In order to have a clear analysis of the data, several criteria for the selection of nuclear levels and transitions to be studied must be fulfilled. First, the level must be principally (90–100 %) populated by a primary gamma ray and not by gamma-ray cascades to induce a well-defined recoil energy.[3] If the nuclear state is populated by gamma-ray cascades, the distribution of the recoils of the nucleus becomes complex and hard to reproduce. Second, the lifetime of the nuclear state has to be in the right order of magnitude (from 10^{-13} to 10^{-15} s) such that a measurable fine structure is observable. Last but not least, the transition must have enough intensity to be analyzed by the GAMS4 spectrometer.

III. SLOWING-DOWN THEORIES AND MD SIMULATIONS

In order to extract the nuclear state lifetime from the crystal-GRID data, molecular dynamics simulations are needed. For the reproduction of the measured gamma-ray line shapes obtained with the GAMS4 spectrometer, the

TABLE I. Reaction and levels used.

Reaction	σ [b]	E_x[a] [keV]	E_γ[a] [keV]	I_γ[a] [%]	$\Sigma I_{in}/\Sigma I_{out}$[a]	τ[a]	Purpose[b]
^{58}Ni$(n,\gamma)^{59}$Ni	4.6	4140.34	3675.23	0.96	100	6.5(1.4) fs	τ
		2414.97	1950.05	1.7	96	53.4(7.2) fs	τ
		339.42	339.42	7.1		98.1(11.5) ps	v_t

[a]Reference 3.

[b]τ, lifetime measurement; v_t, thermal velocity measurement.

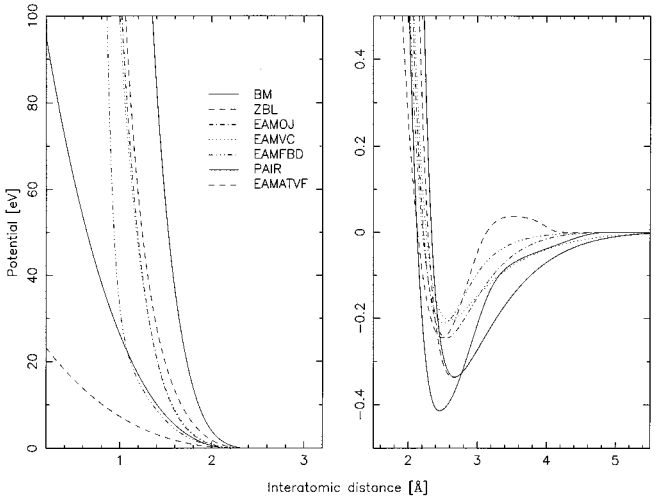

FIG. 2. Theoretical interatomic potentials for the Ni-Ni interaction. All the potentials are placed in the figure from the most (BM) to the least (EAMATVF) repulsive potential.

slowing down of Ni atoms was simulated using a constant-energy and -volume MD program.[5] The MD cells comprised 1372 atoms (6 translations in the *x*, *y*, and *z* directions of a unit cell of 4 atoms), and periodic boundary conditions were applied in all three dimensions. Atoms were placed in a fcc array and are thermalized to the desired temperature by solving numerically the equation of motion using a Verlet algorithm[14] during a few ps. Once thermalization is achieved, an isotropically distributed recoil velocity was imparted to the most central atom in the lattice by adding vectorially the gamma-ray-induced velocity to the thermal velocity. The simulation is then continued with a time step of 0.5 fs until the probability of gamma emission determining the line shape of interest is sufficiently low. Typically, the simulation is performed during 4τ (τ is the lifetime of the excited state). This time interval ensures that 98% of the gamma rays will be emitted due to the exponential decay law. The velocities and positions of a set of recoiling nuclei are stored for future evaluation of the line shape. For the calculation of the gamma-ray line shape, 1500 of such events were simulated.

The dependence of the simulated gamma-ray line shape on the interatomic potential was studied with seven different potentials. A Born-Mayer (BM) (Ref. 15), a ZBL (ZBL) (Ref. 16), a pair (PAIR) (Ref. 17) potential, and four embedded-atom method [EAMFBD (Ref. 12), EAMVC (Ref. 18), EAMOJ (Ref. 19), and EAMATVF (Ref. 20)] potentials were investigated using molecular dynamics simulations. Figure 2 shows the seven potentials used in this work. A detailed description of those is given in Appendixes A and B. The values of the different parameters used for the determination of the interatomic potentials are listed in Tables II and III. All potentials are analytically simple to be implemented in the computer code and are mainly dependent on the interatomic distances (r_{ij}) between atoms *i* and *j*. The three first well-known potentials are described in Appendix A.

Potentials derived using more recent theories, which describe the interaction between atoms in a solid by the so-called embedded atom method introduced by Daw and Baskes,[21] were also investigated. The basic idea of the EAM potentials is that the electron density in a metal can be approximated by a superposition of the electron densities of individual atoms. The electron density near an atom is determined by the electron density of that atom plus a background electron density from the other atoms. Therefore each atom can be thought of as being embedded in the electron density of the surrounding atoms. In this approach, the total energy is modeled by a sum over all atoms as having two contributions: the energy to embed an atom into the local electron density provided by the remainder of the atoms and an electrostatic interaction represented by a pair potential that accounts for the core-core repulsion. The total energy is written as

$$U=\sum_i F_i(\rho_i)+\frac{1}{2}\sum_{i\neq j}\Phi_{ij}(r_{ij}), \tag{3}$$

where F_i is the energy required to embed atom *i* in the background electron density and Φ_{ij} is the short-range pair interaction representing the core-core repulsion between atom *i* and *j* with interatomic separation r_{ij}. The host electron density (ρ_i) at the position of atom *i* is approximated by the superposition of the atomic electron density (ρ_j^a) of the neighbors *j* by

$$\rho_i=\sum_j \rho_j^a(r_{ij}). \tag{4}$$

In order to apply this method, the embedding functions $F_i(\rho)$, pair repulsion Φ_{ij}, and atomic density $\rho_i(r)$ must be known. By assuming reasonable functional dependencies for the pair potential, the atomic electron density, and the embedding function, these functions can be fitted to yield the known lattice constant, elastic constants, vacancy formation energy, and sublimation energy of a perfect homonuclear crystal. Many forms for the different functions needed have been developed in the last years for nickel crystals and are summarized in Appendix B.

To simplify the determination of the total energy given by Eq. (3) and the interatomic potential in the MD simulation, an effective pair potential was used. The effective pair potential reduces considerably the calculation of the EAM po-

TABLE II. Repulsive potentials parameters for nickel.

BM	ZBL	PAIR
$A=132\ 71$ eV	$c_1=0.02817$	$b=3.52$ Å
$B=0.280\ 25$ Å	$c_2=0.28022$	$\phi(0.6b)=0.0504$ eV
	$c_3=0.50986$	$\phi(0.7b)=-0.4138$ eV
	$c_4=0.18175$	$\phi(0.8b)=-0.3078$ eV
		$\phi(0.9b)=-0.1415$ eV
	$d_1=0.20162$	$\phi(1.0b)=-0.0715$ eV
	$d_2=0.40290$	$\phi(1.1b)=-0.0455$ eV
	$d_3=0.94229$	$\phi(1.2b)=-0.0245$ eV
	$d_4=3.19980$	
		$r_c=4.841$ Å
	$x=0.23$	$\phi(r_c)=0.0$ eV
	$y=-1.0$	$\phi'(0.6b)=-3.620$ eV/Å
		$\phi'(r_c)=0.0$ eV/Å

TABLE III. EAM potentials parameters for nickel.

EAMFBD	EAMVC	EAMOJ	EAMATVF
$a_1 = 0.070\,937$[a]	$D_m = 1.5335$ eV	$\beta = 6$	$a_1 = 29.057\,09$ eV
$a_2 = 0.146\,031$[a]	$\alpha_M = 1.7728$ Å^{-1}	$\gamma = 9$	$a_2 = -76.046\,25$ eV
$r_c = 3.0045$ Å	$\beta_M = 3.6408$ Å^{-1}	$\delta = 20$	$a_3 = 48.089\,20$ eV
	$R_M = 2.2053$ Å	$r_c = 4.729$ Å	$a_4 = -25.966\,04$ eV
$F(0.0$ Å$^{-3}) = 0.0$ eV	$r_c = 4.7895$ Å	$\phi_e = 0.63199$ eV	$a_5 = 79.151\,21$ eV
$F(0.014\,46$ Å$^{-3}) = -3.5847$ eV		$a = -3.1684$	$r_1 = 4.311\,102\,1$ Å
$F(0.028\,91$ Å$^{-3}) = -5.1449$ eV		$b = -5.1237$	$r_2 = 4.064\,563\,0$ Å
$F(0.057\,83$ Å$^{-3}) = -3.4041$ eV		$n = 0.12501$	$r_3 = 3.935\,382\,9$ Å
$F(0.066\,50$ Å$^{-3}) = 0.0$ eV		$\rho_e = 12.551$ Å^{-3}	$r_4 = 3.520\,000\,0$ Å
			$r_5 = 3.048\,409\,4$ Å
			$A_1 = 60.537\,985$ eV
			$A_2 = -80.102\,414$ eV
			$R_1 = 4.311\,102\,1$ Å
			$R_2 = 3.935\,382\,9$ Å

[a]Value expressed in electron charge units.

tential as this method permits us to consider the different EAM potentials as pair potentials. In an approach developed by Foiles *et al.*,[7] the EAM energy can be approximated as an effective pair potential by expanding the embedding functional in a Taylor series around the equilibrium electron density $\overline{\rho}$ and dropping three-body and higher-order terms. The effective total energy $E_{\rm tot}$ and effective pair potential $\Psi(r)$ are then given by

$$E_{\rm tot} \approx N[F(\overline{\rho}) - \overline{\rho}F'(\overline{\rho})] + \frac{1}{2}\sum_{\substack{i,j \\ i \neq j}} \psi(r_{ij}), \tag{5}$$

$$\psi(r) = \phi(r) + 2F'(\overline{\rho})\rho^a(r) + F''(\overline{\rho})[\rho^a(r)]^2, \tag{6}$$

where $F'(\overline{\rho})$ and $F''(\overline{\rho})$ denote the first and second derivatives of the embedding energy with respect to the local electron density ρ and N the total number of atoms. The equilibrium electron densities used in the present work are 0.028, 0.38, 12.55, and 37.41 Å^{-3} for the EAMFBD, EAMVC, EAMOJ, and EAMATVF potentials, respectively. The large difference in $\overline{\rho}$, $\rho(r)$, and $F(\rho)$ is due to the different procedures used for reproducing the solid-state and bulk-metal properties.

Once the recoiling atom velocities and positions have been recorded following the MD simulations according to the selected potential, the gamma-ray-induced Doppler-broadening line shape can be calculated by the formula

$$I(E) = C\sum_i \int_0^\infty e^{-t/\tau}\delta\left[E - E_\gamma\left(1 + \frac{\mathbf{v}_i(t)\cdot\mathbf{n}}{c}\right)\right]dt, \tag{7}$$

where C is a normalization constant, τ the excited-nuclear-state lifetime, E_γ the nonshifted energy of the transition, $\mathbf{v}_i(t)$ the velocity vector of the ith simulated atom at the moment of emission as calculated by the MD programs, $\mathbf{n}$ the relative direction of observation, and c the velocity of light. The index (i) ranges generally from 1 to 1500 and represents the number of recoil events calculated by the molecular dynamics simulations. The natural linewidth is neglected in the calculation of the line shape since its effect contributes to less than 1% of the total broadening.[5] The exponential term in formula (7) expresses the lifetime dependence of the line shape and the last term the Doppler broadening due to the velocity of the emitting nucleus. In formula (7), the integration goes from 0 to ∞, because the gamma ray can be emitted at anytime due to the decay law probability, but in the present work, the integration was cut at 4τ to restrain the simulation time as explained above.

At the moment of emission the velocities of the atom and gamma-ray directions are fixed by the molecular dynamics simulations and by the crystal orientation with respect to the GAMS4 spectrometer, such that the gamma-ray line shape can be evaluated for different lifetime values (τ). These line shapes are then fitted to the measured data using the least-squares fitting routine GRIDDLE,[22] with the lifetime and experimentally related numbers (background, intensity, etc.) as free parameters. As a result of this procedure, a lifetime value τ and a χ^2 per degree of freedom are obtained. Both values permit one to quantify the agreement or disagreement between theory (MD simulation of the slowing down) and experiment (crystal-GRID data).

IV. GAMMA-RAY-INDUCED DOPPLER-BROADENING MEASUREMENTS

A. Experiment

fcc single crystals of Ni in its natural isotopic composition were used for the experiment. The density of the single crystal is 8.908 g/cm^3 and the fcc lattice constant is equal to 3.52 Å.[23] Two different orientations of the crystal planes with respect to the spectrometer, the [100] and the [111], were analyzed. In both measurements, three $2\times20\times25$ mm^3 single crystals of Ni were irradiated at the in-pile target position of the ILL high-flux reactor in a neutron flux of 5×10^{14} cm^{-2} s^{-1}. The crystal orientations were checked with back-reflection Laue pictures created by x-ray irradiation[24] before beginning the experiments. The crystals were then inserted in graphite holders and placed inside the reactor. The orientation uncertainty is determined by the precision of the crystal cut and of the positioning system inside the reactor and is equal to $\pm 2.0°$. For the measurements of the Dop-

pler profiles, the ultrahigh resolution of the GAMS4 spectrometer was used. This two-axis flat-crystal spectrometer allows measurement of gamma-ray broadening in the order of $\Delta E/E = 10^{-4} - 10^{-6}$,[25] using twice the Bragg law to select the correct energy. The first crystal is set to the Bragg angle for a given energy. The second crystal is then rocked around this angle, and the gamma intensity is measured for each position with a germanium detector. For the [111] orientation, besides the full energy peak, the single- and double-escape peaks in the germanium spectrum were also considered for the analysis of the highest-energy transition. The GAMS4 spectrometer can operate under two modes: a nondispersive mode denoted by (n,n), where n is the order of reflection, by setting the two crystals parallel to each other, and a dispersive mode denoted by $(n,-m)$ by turning the second crystal to its mirror position with respect to the incident gamma ray with $m=n$ or to any angle suited for mth-order diffraction on the second crystal with $m \neq -n$.[1,25] The nondispersive mode allows one to experimentally determine the instrumental response. This is well described by dynamical diffraction theory folded with a small Gaussian with a full width at half maximum which is called the excess width (ew). The dispersive mode is used to measure the Doppler-broadened line shapes.

B. Measurement of the broadening due to thermal motion

The thermal broadening related to the target temperature inside the nuclear reactor is determined with the 339-keV nuclear state. As this level has a very long lifetime (98.1 ps) compared to the slowing-down time, the nucleus has sufficient time to thermalize before the emission of the observed gamma ray. Therefore the only Doppler broadening the gamma ray will undergo is the one due to thermal motion. The spectrometer response function was first determined in the second order, and then the dispersive mode gives a thermal velocity of 532(40) m/s in the third order. The third order of reflection was not measured in the nondispersive mode to reduce the measuring time, because the ew does not depend on the order of reflection and the intensity decreases with higher orders of reflection.[25] Figure 3 shows the line shape obtained for the 339-keV transition in both dispersive and nondispersive modes for the [100] orientation. The effective temperature corresponding to the mentioned thermal velocity is equal to 666(101) K. The present thermal velocity is consistent with the velocity obtained with polycrystalline targets under the same irradiation conditions.[26] The temperature value of 666 K was adopted for the thermalization of the cell in all molecular dynamic simulations performed in this work. Note that this imposes the same Maxwellian distribution on the simulation as the one measured.

C. Measurement of the gamma-ray-induced Doppler broadening

Two transitions were chosen to investigate the influence of the potential and the effects due to the target orientation on the line shape. The 3675- and 1950-keV transitions allow one to study the motion of the emitting ^{59}Ni after the emission of a primary gamma ray of 4854 and 6884 keV, respectively. The 2415-keV nuclear level and its 1950-keV transition were selected because the lifetime was known by several

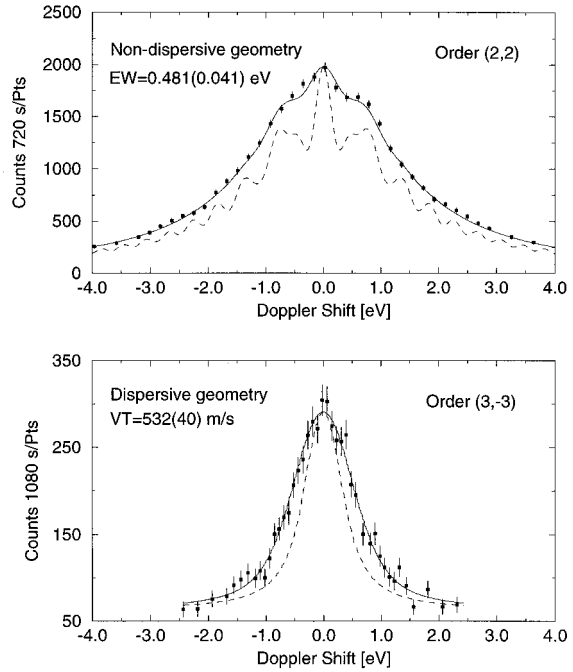

FIG. 3. Gamma-ray line shape of the 339-keV transition in dispersive and nondispersive geometry. In the upper part, the dotted line represents the diffraction theory curve and the solid line exhibits the diffraction theory curve folded with a fitted excess width. In the lower part, the dotted line corresponds to the instrumental response (calculated by nondispersive scans; note that the reflection order is not the same for both modes) and the solid line is the line shape fit representing the given thermal velocity value.

other methods,[3] which permits the selection of the interatomic potential by the value obtained for the nuclear lifetime. The 4140-keV level with its 3675-keV transition has a smaller lifetime, and the influence of the target orientation on the structure should be more obvious. However, the lifetime mentioned in the literature was only measured by the GRID method. Therefore the selection of a potential by checking the lifetime cannot be made directly with only this transition. Before measuring the gamma-ray-induced Doppler-broadening profile giving a value for the lifetime with the aim of the MD simulations, the instrumental response function for the transition has to be known. The fitted excess width for both transitions and for both orientations was determined by the dispersive mode of the 1950-keV transition in second order of reflection and is set to 9.41(0.51) marcsec for the [100] and 9.94(0.76) marcsec for the [111] orientation. Figure 4 shows the nondispersive line shape obtained for the 1950-keV transition in the [100] orientation.

V. DATA ANALYSIS AND RESULTS

The fitted lifetime values extracted using seven potentials are summarized in Tables IV and V and are illustrated in Fig. 5. For comparison, the most recent adopted values for the lifetime of the nuclear states measured by other methods[3,4,27(a),27(b),28] are also shown in the figure.

The measurement proves that the gamma-ray line shape depends strongly on the orientation of the target with respect to the GAMS4 spectrometer. The Doppler-broadened line shape is thus indeed correlated for short lifetimes to the or-

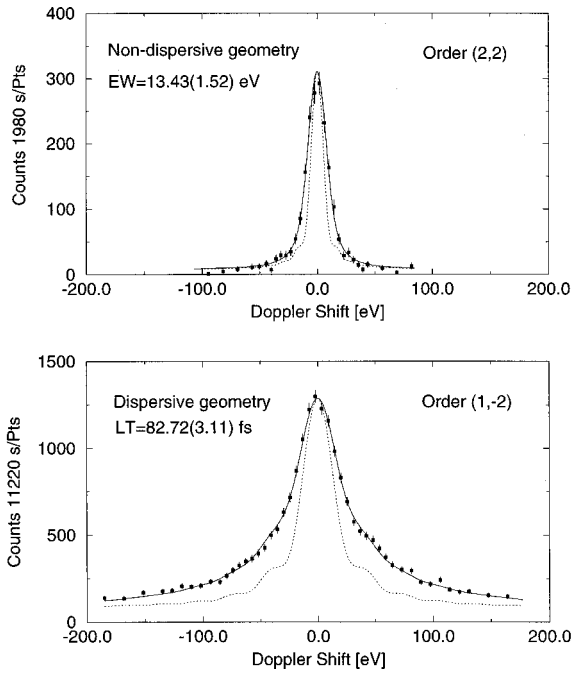

FIG. 4. Gamma-ray line shape of the 1950-keV transition in nondispersive second-order (top) and dispersive third-order (bottom) geometry. In the upper part, the dotted line represents the diffraction theory curve and the solid line corresponds to the diffraction theory curve folded with a fitted excess width. In the lower part, the dotted line corresponds to the instrumental response (calculated from nondispersive scans; note that the reflection order is not the same for both parts) and the solid line corresponds to the line shape fit for the given lifetime value. In order to have the same scale in both parts, the ew was converted into eV in the upper part of the figure.

dering of atoms in the crystal. The difference in the gamma-ray structure is shown in Fig. 6 for the 3675-keV transition in the [111] and [100] orientations. Also shown is the fit obtained from MD simulations using the EAMVC potential. On average, the atom moving towards the [111] direction has more freedom due to the positions of the neighboring atoms and the slowing down in this direction is less pronounced. The resulting line shape is therefore more broadened as can be seen by comparison with the line shape obtained from the [100] direction in Fig. 6.

Figure 7 shows the fitted line shape obtained for the [100] orientation using three distinct potentials. Although the gamma-ray line structure is relatively close for these three potentials, there are huge differences in the fitted lifetime value. By comparing the fitted lifetime (Tables IV and V) with the form of the interatomic potential (Fig. 2), one can conclude that the more repulsive the potential is, the smaller the lifetime becomes. With a highly repulsive potential, the slowing down of the recoiling atom takes place more rapidly, which decreases the fitted lifetime in order to have the same Doppler broadening. (A smaller lifetime increases the Doppler broadening, as more gamma rays will be emitted due to the exponential decay law with greater velocities). As the 4140-keV nuclear-state lifetime obtained with the EAMVC and the EAMOJ potentials are very similar, 7.8(0.5) and 7.9(0.6) fs, one might expect that the forms of these two interatomic potentials are identical. This is the case for the repulsive part, but not for the form of the potential at equilibrium distance (see Fig 2), which indicates that in the particular case of nickel the attractive form of the interatomic potential does play a minor role in the calculation of the gamma-ray line shape for a slowing-down energy in the order of a few hundred of eV and lifetimes in the fs range. To illustrate the differences in line shapes obtained from the MD simulations, the lower part of Fig. 7 shows the profiles calculated for a given lifetime $\tau = 7$ fs.

The lifetime of the 2415-keV nuclear state deduced from the data using the MD simulations can be used to judge the reliability of interatomic potentials. If a MD potential can reproduce the lifetime measured by several other nuclear methods, then it will be suited for a description of the slow-

TABLE IV. ^{59}Ni nuclear-state lifetimes obtained using the different potentials fitted to the GAMS4 data. For the potentials names, refer to Appendix A.

E_x [keV]	E_γ [keV]	Orientation [xyz]	Order (n,m)	Number of scans	BM lifetime [fs]	ZBL lifetime [fs]	PAIR lifetime [fs]
4140.34	3675.23	[100]	(1,−1)	12	3.6(0.4)	5.7(0.8)	22.4(7.2)
			(1,−2)	16	5.6(0.8)	9.5(1.5)	>50[c]
			Both	28	4.1(0.4)	6.7(0.7)	32.5(10.7)
		[111]	(1,−1)	15	4.1(0.4)	6.7(0.8)	29.6(10.9)
			(1,−2)	17	6.0(1.2)	8.5(1.9)	>50[c]
			Both	32	4.4(0.4)	7.1(0.7)	38.1(13.8)
		Both[a]	Both		4.2(0.4)	6.9(0.5)	35.3(8.7)
2414.97	1950.05	[100]	(1,−1)	7	28.9(3.1)	52.5(5.5)	>200[c]
			(1,−2)	34	25.0(1.0)	44.0(1.8)	>200[c]
			Both	41	25.7(1.0)	45.4(1.7)	>200[c]
		[111]	(1,−2)	12	29.9(2.6)	53.4(4.6)	>200[c]
		Both[a]	Both[b]		26.2(1.0)	46.3(1.6)	>200[c]

[a]Weighted average from the two orientations, not a fit.

[b]Weighted average from the two orientations, not a fit: [100] two orders, [111] one order.

[c]Lifetime fit not convergent, lower limit (see text).

TABLE V. ^{59}Ni nuclear-state lifetimes obtained with different embedded-atom method (EAM) potentials using the MD simulations fitted to the GAMS4 data. For the potentials names, refer to Appendix B.

E_x [keV]	E_γ [keV]	Orientation [*xyz*]	Order (*n*,*m*)	Number of scans	EAMOJ lifetime [fs]	EAMVC lifetime [fs]	EAMFBD lifetime [fs]	EAMATVF lifetime [fs]
4140.34	3675.23	[100]	(1,−1)	12	6.4(0.9)	6.5(.9)	9.6(1.4)	>100[c]
			(1,−2)	16	10.9(1.8)	11.2(1.9)	17.9(4.0)	>150[c]
			Both	28	7.6(0.8)	7.7(0.8)	11.5(1.3)	>150[c]
		[111]	(1,−1)	15	7.6(0.9)	7.7(0.9)	11.5(1.6)	>100[c]
			(1,−2)	17	9.7(2.2)	9.9(2.2)	15.6(4.9)	>150[c]
			Both	32	8.0(0.8)	8.2(0.8)	12.3(1.4)	>150[c]
		Both[a]	Both		7.8(0.5)	8.0(0.6)	11.9(1.0)	>150[c]
2414.97	1950.05	[100]	(1,−1)	7	58.1(6.1)	60.3(6.3)	102.3(13.9)	>300[c]
			(1,−2)	34	49.0(1.9)	50.4(2.0)	92.0(4.6)	>250[c]
			Both	41	50.4(1.9)	51.9(1.9)	93.5(4.3)	>300[c]
		[111]	(1,−2)	12	57.6(4.9)	61.6(5.3)	98.0(10.6)	>400[c]
		Both[a]	Both[b]		51.3(1.7)	53.1(1.8)	94.2(4.0)	>400[c]

[a]Weighted average from the two orientations, not a fit.
[b]Weighted average from the two orientations, not a fit: [100] two orders, [111] one order.
[c]Lifetime fit not convergent, lower limit (see text).

ing down of atoms in the given energy range. For the 4140-keV level studied in this work, this is not possible because the lifetime was only measured by the GRID method and by the present crystal-GRID approach. Therefore no direct conclusion on the potential can be made with this only level. Both independent measurements reproduce, however, the same consistent lifetime values (6.5–8.9 fs) if the same slowing-down theory is used.[2,4] For the two least repulsive potentials, namely, the EAMATVF and PAIR potentials, the fitted lifetime is 5–8 times higher than the literature value[3] (confer Tables IV and V). In these two cases, the fitted life-

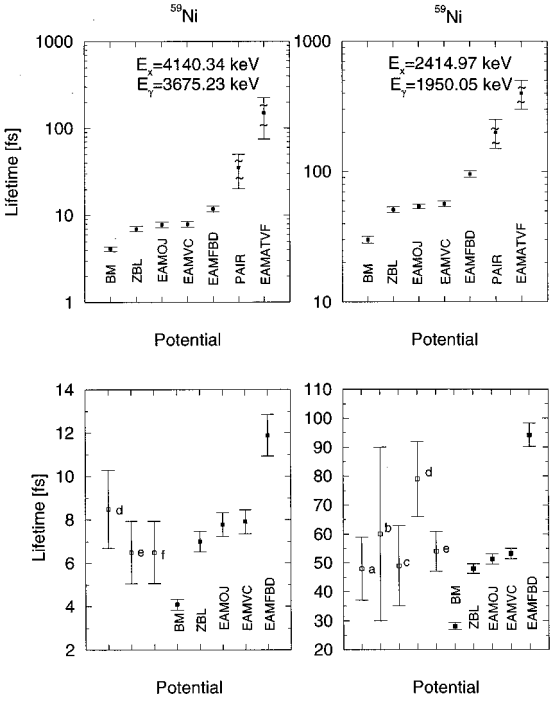

FIG. 5. Lifetime values simulated with the different slowing down potentials for the 4140- and 2415-keV nuclear-state levels. The lower part shows the comparison of the lifetime value with the lifetime found in the literature: (a) Ref. 27(a), (b) Ref. 27(b), (c) Ref. 28, (d) Ref. 2, (e) Ref. 4, and (f) Ref. 3. The solid squares represent the new crystal-GRID measurements and the open squares the published lifetime measurements.

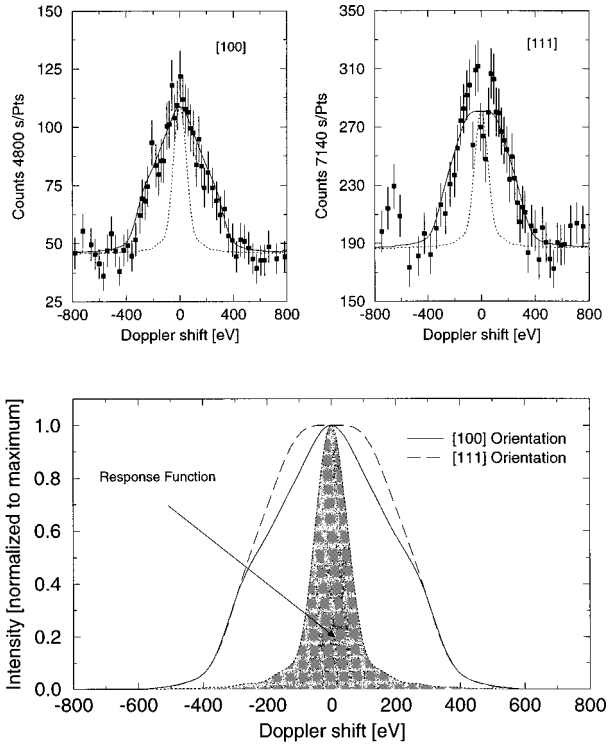

FIG. 6. Gamma-ray line shape of the 3675-keV transition in the (1,−2) order of reflection in the [100] and [111] orientations. The experimental line shapes are obtained from a summation of ~16 individual scans. They are based on the full energy peak only. The lower part shows the fitted line shape for both orientations with the maximum intensity normalized to 1.0.

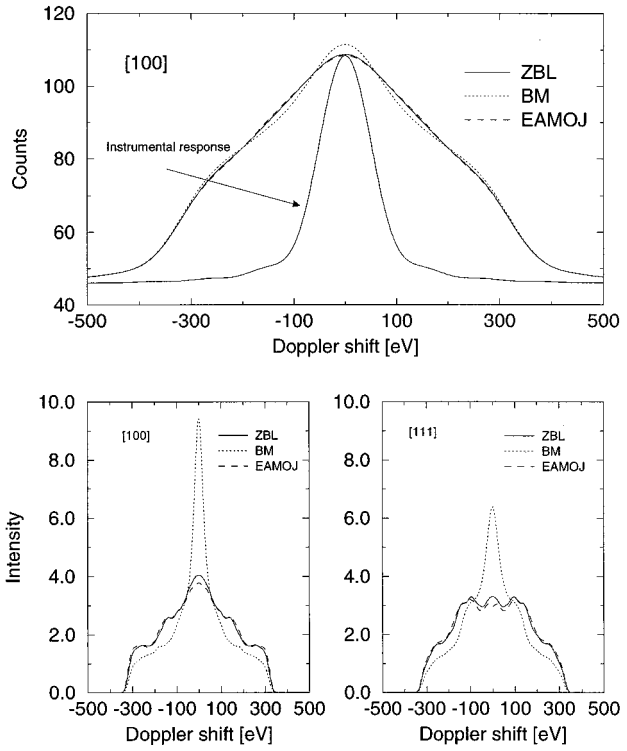

FIG. 7. The upper part shows the gamma-ray line shape for the ZBL, BM, and EAMOJ potentials calculated with the MD programs and fitted to the crystal-GRID data for the 3675-keV transitions for the [100] orientation. The lower part shows the simulated line shape for both orientations for a given lifetime value $\tau=7$ fs. To have a better view of the structure, the instrumental response function was intentionally set to a small (10.0 eV) value, compared to the measured one (see upper part).

time becomes very long and the program GRIDDLE does not converge towards a final result after several iterations. As the simulation time interval, defined as the time needed to follow the recoiling atom, was set before the fit to 75 fs ($\sim 4\tau_{\max}$, the maximum expected lifetime) for the 4140-keV nuclear state, the exponential decay law gives rise to problems when the fitted lifetime increases well beyond this estimated value. As the number of gamma rays emitted after the predefined $4\tau_{\max}$ simulation limit increases, the contribution of these gamma rays cannot be neglected and the line shape is perturbed. However, as the fitted lifetime value is far above the literature value, no new longer MD simulations were performed. The best interatomic potentials determined by the crystal-GRID method for the slowing down of Ni atom in a fcc Ni single crystal are the ZBL, EAMVC, and EAMOJ potentials. The 2415-keV nuclear-state lifetime value obtained with these potentials agrees quite well with the one given in the literature[3] and measured by other methods. These three potentials also give the best χ^2 per degree of freedom (see Table VI), which tends to prove that they are the most appropriate. The lifetime for the 4140-keV state measured with the present approach is also consistent with previous polycrystalline GRID measurements.[2]

In order to cross-check the reliability of the EAMVC and EAMOJ potentials, an optimization of the ZBL potential was tested. This was done by performing MD simulations with different x parameters defining the ZBL potential [see Eq. (A4) in Appendix A] and by fitting the GAMS4 data for the 3675-keV transition. As the form of the ZBL potential is relatively close to the other EAM potentials, the change in the ZBL potential should tend towards the EAM potential if these two are correct. The fitted lifetime and the χ^2 per degree of freedom are then a measure of improvement or aggravation of the description of the line shape. The smallest χ^2, which ensures the best fit to the data, is obtained for an x parameter of 0.26. This x parameter produces a lifetime value of 8.6(0.9) fs for the [111] and a lifetime of 8.2(0.8) fs for the [100] orientation. Figure 8 shows the change in the simulated line shape obtained with the ZBL potential for different x parameters as well as the resulting potential for given parameter values. The variation of the χ^2 value is illustrated in Fig. 9 for both orientations. The dependence of

TABLE VI. χ^2 per degree of freedom for the different potentials for the 4140-keV fitted nuclear state lifetime.

Slowing down	χ^2_{abs}[100][a]	χ^2_{abs}[111][a]	Lifetime [fs]	χ^2_{mean} [b]
BM	1810.89	2015.67	4.2(0.4)	1.1385
ZBL	1808.96	2012.90	6.9(0.5)	1.1371
EAMFBD	1809.22	2013.45	11.9(1.0)	1.1374
EAMOJ	1809.19	2013.24	7.8(0.5)	1.1373
EAMVC	1808.80	2012.97	8.0(0.6)	1.1371

[a]Absolute χ^2. The number of degree of freedom (N_{freedom}) for the lifetime χ^2 is equal to 1595 and 1766 for the [100] and [111] orientations, respectively.

[b]Mean χ^2 per degree of freedom taken from both orientations as $\Sigma\chi^2_{\text{abs}}/\Sigma N_{\text{freedom}}$.

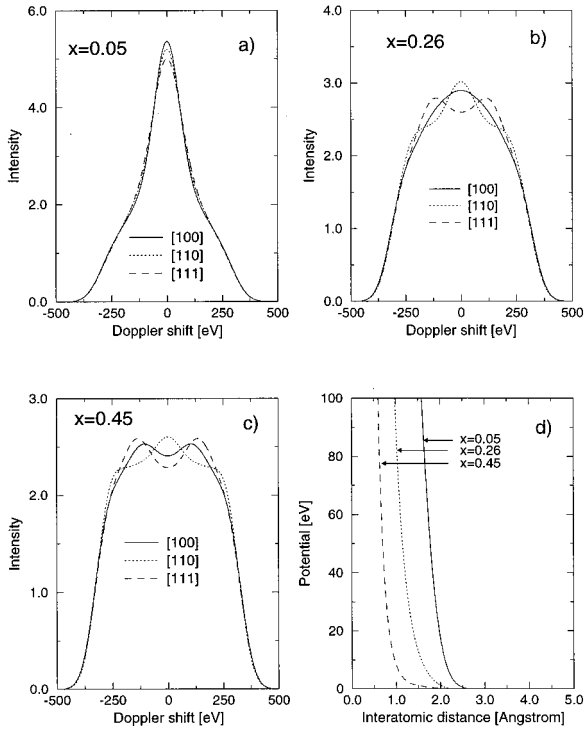

FIG. 8. Simulated line shape obtained with a given lifetime of $\tau=7$ fs for three different x parameters (a), (b), (c). Here (d) shows the variation of the ZBL potentials for the given parameters. For the explanation of the x parameter, see Eq. (A4) in Appendix A.

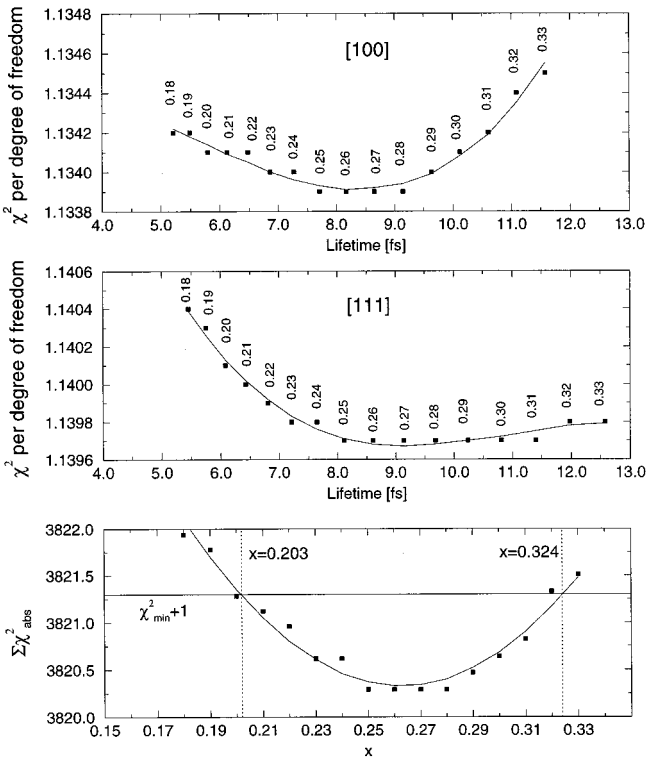

FIG. 9. χ^2 per degree of freedom vs fitted lifetime for the different x parameters. The x values are listed above the point. The function shows a minimum for $x=0.26$. The solid line represents a cubic polynomial interpolation of the points. The lower part gives the absolute χ^2 vs the x parameter. The absolute χ^2 is obtained by adding the absolute χ^2 of both orientations.

the χ^2 versus the lifetime is asymmetric due to fit related phenomena. As the measured line shape is fixed, the MD-simulated line shape has to be fitted to the data mainly by adjusting the lifetime value. However, the simulated line shape has also a structure which cannot be changed enormously by the lifetime value. For instance, the line shapes simulated for the [100] orientation with $x=0.05$ and $x=0.45$ differ greatly. Once the maximum value is at the center, and once a pseudominimum occurs at the center of the line shape (see Fig. 8). As the measured GAMS4 line shape has a maximum at the middle (see Fig. 7), the line shape simulated with the $x=0.05$ will be easier to fit to the data than the line shape simulated with $x=0.45$ will. This results in a smaller χ^2 per degree of freedom for smaller x despite the fact that the lifetime value diverges from the correct value for x parameters away 0.26. Therefore an asymmetry arises in the mentioned function. The lower part of Fig. 9 shows the summed χ^2 for both orientations. From these, it can be deduced that the fitted x value has an error of ± 0.06. If the lifetime were precisely known, this error could be reduced by the constraint that the x parameter also reproduce the exact τ.

The best x parameter was then used to simulated the other transition (1950 keV), and it gives a lifetime of 54.2(1.9) fs. The new parameter of the ZBL potential gives thus a lifetime very close to the EAMVC and EAMOJ values, and if one looks at the form of the new ZBL potential, it resembles closely the form of the two embedded-atom potentials (see Fig. 10). This reinforces the fact that the two embedded-atom

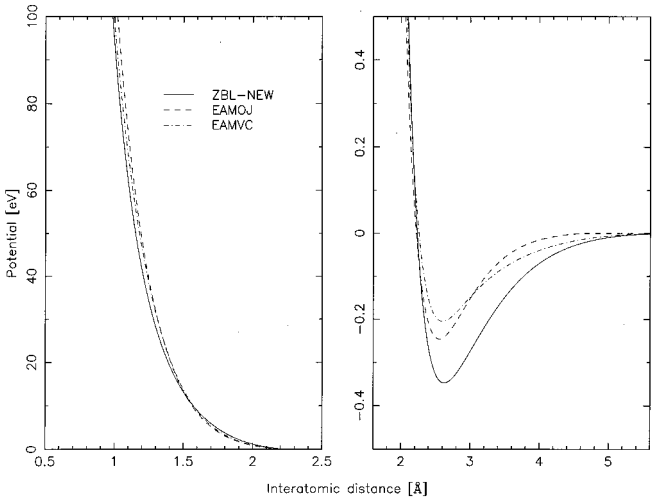

FIG. 10. Comparison of the modified ZBL (ZBL-NEW) interatomic potential ($x=0.26$ instead of 0.23; see Table II) with the two EAM potentials. The main difference is at equilibrium distance.

method potentials are the best for the parametrization of the interatomic slowing down in fcc nickel crystals at a few hundred of eV.

All the errors given in the preceding tables are only least-squares errors on the fitted lifetime. They do not include the small statistical error made in the calculations of the excess width which is used for the lifetime determination. The statistical error coming from the MD simulations, correlated to the number of MD recoiling events, was also left out. The influence of statistical errors (from the measurements and from the MD simulations) is given in Table VII for the EAMOJ slowing-down theory. The final result, obtained with the EAMOJ potential, returns a value of 7.7(0.9) fs for the 4140-keV nuclear state.

VI. CONCLUSION

The influence of the form of the interatomic potentials on recoiling Ni atoms in fcc Ni crystals at an energy of 200–400 keV was investigated by measuring the lifetime value of two nuclear levels. The selection of two best embedded-atom method potentials [EAMVC (Ref. 18) and EAMOJ (Ref. 19)] among seven different potentials investigated by the crystal-GRID method was possible. A new ZBL potential was deduced from this analysis. The convergence of the modified ZBL potential toward the EAMVC and EAMOJ potentials tends to corroborate our choice for these two potentials as the best candidates. The smallest χ^2 per degree of freedom obtained with these potentials proves that the two embedded-atom potentials cannot only reproduce solid-state constants quite well, but are also reliable on the slowing down of atoms with energy in the order of 200 eV in bulk material.

It was also shown that the measured line shape depends strongly on the orientation of the target with respect to the GAMS4 spectrometer when single crystals are used. This confirms that crystal-GRID measurements are preferable, when possible, over GRID measurements.

The lifetime values obtained for the two transitions have a higher precision than all previous measurements. The final

TABLE VII. Statistical errors on the 4140-keV nuclear-state lifetime obtained with the EAMOJ potential depending on recoil numbers and on the experimental error made in the measurements of the excess width.

Value used in the fit		Number of MD recoils	Orientation [100] lifetime [fs]	Orientation [111] lifetime [fs]
(1)	ew	250	7.6(0.8)	8.3(0.8)
	ew	500	7.4(0.8)	8.8(0.8)
	ew	750	7.2(0.8)	8.8(0.8)
	ew	1000	7.5(0.7)	8.2(0.8)
	ew	1250	7.4(0.7)	8.1(0.8)
	ew	1500	7.6(0.8)	8.0(0.8)
	ew	1500	7.6(1.1)[a]	8.0(1.6)[a]
(2)	ew+dew	1500	7.6(0.8)	8.1(0.8)
	ew−dew	1500	7.5(0.7)	8.0(0.8)
(3)	ew	1500	7.6(1.1)[b]	8.0(1.6)[b]
	ew	1500	7.7(0.9)[c]	

[a]Biggest statistical error. $LT_{\text{mean}}+/-(LT_{\text{max/min}}+/-dLT)$. Example [100]: $7.56-(7.21-0.75)=1.10$.
[b]Biggest statistical error from simulations (1) and (2).
[c]Weighted average from both orientations using the error calculated in (3).

result with the EAMOJ potential yields a value of 7.7(0.9) fs for the 4140-keV nuclear-state level and a value of 51(3) fs for the 2415-keV nuclear state including both statistical and MD simulation errors. These lifetimes are consistent with the values given in the literature.

ACKNOWLEDGMENTS

This work was supported by the Swiss National Research Fund. The authors are especially grateful to Dr. A. Voter of Los Alamos National Laboratory for providing useful information for the use of the EAMVC potential.

APPENDIX A

Here we present the different formulas needed to describe the BM, ZBL, and PAIR interatomic potentials. For the values of the different parameters for nickel, refer to Table II in the main text. The Born-Mayer pair potential has been obtained by Abrahamson[15] by fitting an exponential function to the results of Thomas-Fermi-Dirac calculations based on the overlapping of the electron clouds and has the form

$$V(r_{ij})=A_{\text{BM}}e^{-r_{ij}/B_{\text{BM}}}, \tag{A1}$$

with the two Born-Mayer parameters listed in Table II.

One of the most used potentials in stopping power calculations at keV energies has been derived by Ziegler *et al.*[16] by fitting a universal function to a large number of calculations for individual atoms pairs. This potential is given by

$$V(r_{ij})=\frac{e^2}{4\pi\varepsilon_0}\frac{Z_iZ_j}{r_{ij}}\Phi(r_{ij}), \tag{A2}$$

where the screening function Φ has the form

$$\Phi(r_{ij})=\sum_{l=1}^{4} c_l \exp\left(\frac{d_l r_{ij}}{a_s}\right) \tag{A3}$$

and the screening length a_s is defined by

$$a_s=0.8853a_B(Z_i^x+Z_j^x)^y, \tag{A4}$$

with $a_B=0.529$ Å the Bohr radius and $Z_{i,j}$ the atomic number of the atoms i and j, respectively. All the needed parameters (c_l,d_l,x,y) for the evaluation of the ZBL potential are listed in Table II.

As these two potentials (BM and ZBL) are only repulsive, the equilibrium positions of atoms corresponding to their lattice sites are obtained by adding an attractive part to the repulsive potential. In the case of nickel and in general for most metals, a Morse potential is used:

$$V_M(r)=D\{e^{-2\alpha(r-r_0)}-2e^{-\alpha(r-r_0)}\}, \tag{A5}$$

with $D=0.4205$ eV, $\alpha=1.4199$, and $r_0=2.480$ Å taken from Refs. 29 and 23 for nickel.

The total interatomic potential is calculated by connecting the attractive and repulsive parts to obtain a smooth total interatomic potential using the formula[2]

$$V(r)=[1-f(r)]V(r)+f(r)V_M(r), \tag{A6}$$

with the attenuation factor $f(r)$ given by

$$f(r)=\frac{1}{1+e^{b(r-r_1)}}, \tag{A7}$$

with $b=5.0\,\text{Å}^{-1}$ and $r_1=1.9$ Å. They are chosen in such a way that the repulsive potential is not affected above a threshold value and that the Morse potential is not changed at the equilibrium position.

The basic method to calculate the pair potential (PAIR) developed by Baskes and Melius[17] involves the selection of a functional form with a number of free parameters for the potential and the variation of the parameters so that the various calculated quantities agree (in a least-squares sense) with the corresponding experimental data. A simple form, expressed by a cubic spline between a number of fixed-node points, with the nodes as free parameters, was chosen for this potential. The lattice constant, elastic constants, sublimation energy, vacancy formation energy, and migration energy are

used in the fitting procedure to evaluate the node points. The fixed-node points and first derivative values at the end points determining the pair potential[17] are listed in Table II.

APPENDIX B

This appendix describes the embedded-atom method potentials used in the MD simulations. In the EAMFBD method developed by Foiles,[12] the atomic density (ρ^a) is taken from the Hartree-Fock calculations[30] and is given by

$$\rho^a(r)=n_s\rho_s(r)+n_d\rho_d(r), \tag{B1}$$

where n_s and n_d are the number of outer *s* and *d* electrons and ρ_s and ρ_d are the densities associated with the *s*- and *d*-wave functions. The parameters used in the current calculation for the atomic configuration are summarized in Table III. The total number of *s* and *d* electrons, n_s+n_d, is fixed to 10 for nickel. Thus the atomic density depends only on the single parameter n_s. This parameter was determined so to have the proper heats of solution of the alloys. The pair potential is expressed in terms of an effective charge $Z(r)$ such that $\Phi(r)=Z^2(r)/r$. The effective charge is parametrized by the simple polynomial form

$$Z^2(r)=a_1(r_c-r)^3+a_2(r_c-r)^4 \tag{B2}$$

for $r<r_c$ and is zero otherwise. The values of a_1, a_2, and r_c for nickel are listed in Table III. The embedding energies are described by natural splines. The knots used for the spline and the corresponding values of $F(\rho)$ are also given in Table III.

Voter and Chen[18] had developed a similar embedded-atom potential (EAMVC) to the EAMFBD. The difference resides in the pairwise-additive function taken to be a Morse potential of the form

$$\Phi_{ij}(r)=D_M\{1-\exp[-\alpha_M(r-R_M)]\}^2-D_M, \tag{B3}$$

where R_M, D_M, and α_M define the location, depth, and curvature of the minimum, respectively. The density function $\rho(r)$ is given by

$$\rho(r)=r^6[\exp(-\beta r)+2^9\exp(-2\beta r)], \tag{B4}$$

which is a modification of the density of a hydrogenic $4s$ orbital, with the second term added to ensure that $\rho(r)$ decreases monotonically with r over the whole range of possible interaction. The functions and their first derivative are forced to go smoothly to zero at a cutoff distance r_c. The parameters of the two functions are defined in Table III. They were fitted to the same experimental data used in the EAMFBD approach. The EAMVC embedded function $F(\rho)$ is obtained in term of a tabular form.[18]

Oh and Johnson[19] (EAMOJ) developed an approach with simple functional forms which result in fewer parameters to fit and provides easy access for adapting the EAM model. The embedding energy $F(\rho)$ is defined as

$$F(\rho)=a(\rho_i/\rho_e)^n+b(\rho_i/\rho_e), \tag{B5}$$

where

$$\rho_i(r)=\sum_{j\neq i} f(r) \tag{B6}$$

and

$$\begin{aligned} f(r)=&f_e\exp[-\beta(r/r_e-1)]-f_e\exp[-\beta(r_c/r_e-1)]\\ &-\beta f_e\{1-\exp[\delta(r/r_e-r_c/r_e)]\}\\ &\times\exp([-\beta(r_c/r_e-1)]/\delta, \end{aligned} \tag{B7}$$

with r_e the shortest equilibrium distance between two atoms. The pairwise-additive interaction has a similar form and is given by

$$\begin{aligned} \Phi(r)=&\Phi_e\exp[-\gamma(r/r_e-1)]-\Phi_e\exp[-\gamma(r_c/r_e-1)]\\ &-\gamma\Phi_e\{1-\exp[\delta(r/r_e-r_c/r_e)]\}\\ &\times\exp[-\gamma(r_c/r_e-1)]/\delta. \end{aligned} \tag{B8}$$

The nine parameters $(\beta,\gamma,\delta,rc,\phi_e,a,b,n,\rho_e)$ for both embedding and pair potential terms [Eqs. (B5)–(B8)] are listed in Table III.

Ackland, Tichy, Vitek, and Finnis[20] (EAMATVF) used a square-root function for the embedding energy based on the second moment of the density of states. The function for both $F(\rho)$ and $\Phi(r)$ consists of a series expansion with built-in step function $[H(x)]$. The distinct coefficients have been fitted to the experimental data as well as the pressure-volume values calculated from first principles. The functions are defined as follows:

$$F(\rho_i)=-\sqrt{\rho_i}, \tag{B9}$$

where

$$\rho_i=\sum_{j\neq i} f(r_{ij}) \tag{B10}$$

and

$$f(r)=\sum_{k=1}^{2}[A_k(R_k-r)^3H(R_{k-r})]. \tag{B11}$$

The pairwise-additive term $\Phi(r)$ has the form

$$\Phi(r)=\sum_{k=1}^{5}[a_k(r_k-r)^3H(r_{k-r})]. \tag{B12}$$

The Heaviside step function $H(x)$ defined in Eqs. (B11) and (B12) is given by

$$H(x)=\begin{cases}0, & x<0,\\ 1, & x\geqslant 0.\end{cases} \tag{B13}$$

The 14 parameters needed to calculated the different functions for the evaluation of the embedded-atom potential developed by Ackland *et al.* are given in Table III.

[1] H. G. Börner and J. Jolie, J. Phys. G **19**, 217 (1993).
[2] A. Kuronen, J. Keinonen, H. G. Börner, J. Jolie, and S. Ulbig, Nucl. Phys. A **549**, 59 (1992).
[3] C. M. Baglin, Nucl. Data Sheets **69**, 733 (1993).
[4] S. Ulbig, K. P. Lieb, H. G. Börner, B. Krusche, S. J. Robinson, and J. G. L. Booten, Z. Phys. A **338**, 397 (1991).
[5] N. Stritt, J. Jolie, M. Jentschel, and H. G. Börner, Phys. Rev. Lett. **78**, 2592 (1997).
[6] M. Jentschel, K. H. Heinig, H. G. Börner, J. Jolie, and E. G. Kessler, Nucl. Instrum. Methods Phys. Res. B **115**, 446 (1996).
[7] S. M. Foiles, M. I. Baskes, and M. S. Daw, Phys. Rev. B **33**, 7983 (1986).
[8] N. Ting, Y. Qingliang, and Y. E. Yiying, Surf. Sci. **206**, L857 (1988).
[9] M. S. Daw and S. M. Foiles, Phys. Rev. Lett. **59**, 2756 (1987).
[10] J. S. Nelson, E. C. Sowa, and M. S. Daw, Phys. Rev. Lett. **61**, 1977 (1988).
[11] P. Stoltze, K. W. Jacobsen, and J. K. Norskow, Phys. Rev. B **36**, 5035 (1987).
[12] S. M. Foiles, Phys. Rev. B **32**, 7685 (1985).
[13] M. S. Daw, M. I. Baskes, C. L. Bisson, and W. G. Wolfer, *Modeling Environmental Effects on Crack Growth Processes*, edited by R. H. Jones and W. W. Gerberich (Metallurgical Society of AIME, New York, 1986).
[14] D. W. Heermann, *Computer Simulation Methods in Theoretical Physics* (Springer-Verlag, Berlin, 1986).
[15] A. A. Abrahamson, Phys. Rev. **178**, 76 (1969).
[16] J. F. Ziegler, J. P. Biersack, and U. Littmark, *The Stopping and Range of Ions in Solids* (Pergamon, New York, 1985).
[17] M. I. Baskes and C. F. Melius, Phys. Rev. B **20**, 3197 (1979).
[18] A. F. Voter and S. P. Chen, in *Characterization of Defects in Metals*, edited by R. W. Siegel, J. R. Weertman, and R. Sinclair, MRS Symposia Proceedings No. 82 (Materials Research Society, Pittsburgh, 1987), p. 175.
[19] D. J. Oh and R. A. Johnson, J. Mater. Res. **3**, 471 (1988); in *Atomistic Simulation of Materials, Beyond Pair Potentials*, edited by V. Vitek and D. J. Srolovitz (Plenum, New York, 1989).
[20] G. J. Ackland, G. Tichy, V. Vitek, and M. W. Finnis, Philos. Mag. B **56**, 735 (1987).
[21] M. S. Daw and M. I. Baskes, Phys. Rev. Lett. **50**, 1285 (1983).
[22] S. J. Robinson and J. Jolie, computer code GRIDDLE, 1992.
[23] C. Kittel, *Introduction to Solid State Physics*, 5th ed. (Wiley, New York, 1976).
[24] E. Preuss, B. Krahl-Urban, and R. Butz, *Laue Atlas* (Kernforschungsanlage, Jülich, 1974).
[25] E. G. Kessler, G. L. Greene, M. S. Dewey, R. D. Deslattes, H. G. Börner, and F. Hoyler, J. Phys. G **14**, 167 (1988).
[26] J. Jolie, H. G. Börner, and S. J. Robinson, in *Capture Gamma-Ray Spectroscopy*, edited by R. W. Wolf, AIP Conf. Proc. No. 238 (AIP, New York, 1991), p. 189.
[27] M. Pichevar, J. Delaunay, and B. Delaunay, Nucl. Phys. A **224**, 34 (1974), (a) lifetime measured from the 878-keV transition and (b) lifetime measured from the 1189-keV transition.
[28] P. Anderson, L. Ekstrom, and J. Lyttkens, Nucl. Data Sheets **39**, 641 (1983).
[29] L. A. Girifalco and V. G. Weizer, Phys. Rev. **114**, 687 (1958).
[30] E. Clementi and C. Roetti, At. Data Nucl. Data Tables **14**, 177 (1974).